J Mater Sci (2009) 44:985–991
DOI 10.1007/s10853-008-3219-4

Model and analysis of size-stiffening in nanoporous cellular solids

Jun Wang · David C. C. Lam

Received: 19 September 2008 / Accepted: 22 December 2008 / Published online: 13 January 2009

Abstract The size of the struts in nanoporous cellular solids typically has a secondary influence on the stiffness of the solids, but it leads to significant stiffening when it is on the same order as the higher-order material parameter. We examined this size-dependence using the higher-order finite-element method (FEM) in this study. Mathematical analysis showed that the displacement field that satisfies the conventional Lame equation can serve as a displacement field template in higher-order FEM. Benchmarking studies showed that results from simulations of beam bending and rod torsion using this FEM approach were in good agreement with results from analytical solutions and experiments. Using this approach, we showed that the stiffness of cellular solids is strongly affected by the cellular arrangement and the density when the cell size is on the order of the higher-order material parameter and that the stiffening behavior in nanoporous polyimide can be explained using higher-order theory. The FEM results also showed that a porous solid with half the weight can be engineered to become as stiff as a fully dense solid if the porous microarchitecture is tailored to take advantage of higher-order stiffening.

J. Wang
Department of Materials Science, Fudan University, 200433 Shanghai, People's Republic of China

D. C. C. Lam (✉)
Department of Mechanical Engineering, The Hong Kong University of Science and Technology, Clear Water Bay, Kowloon, Hong Kong
e-mail: david.lam@ust.hk

Introduction

Putting holes into a solid reduces the weight but also softens the solid. The elastic modulus of cellular foam is proportional to the elastic properties of the solid (E_S) and to the fourth power of the ratio of the strut size to the cell size (t/l). Adding more cells or making the cells larger reduces the stiffness of the internal struts and the elastic modulus of the foam [1, 2]. The elastic modulus typically varies with the square of the density such that incorporation of 30% random cells into a solid would reduce the relative elastic modulus (E/E_S) of the foam to less than half. If the density is held constant, classical mechanics models and experiments show that the elastic properties are unaffected by the cell size in cellular solids [3].

When the pores are in the nanometer size range, the elastic properties are found to behave differently. Han et al. [4] prepared polyimide nanofoam using a polyimide precursor with grafted-on liable poly(propylene glycol) oligomer. The liable component was eliminated at 300 °C resulting in a nanoporous polyimide with 20–40 nm interconnected pores. Dynamic mechanical analysis indicated that the nanofoam had a higher storage modulus compared to solid polyimide. Similar stiffening of microporous polyimide films produced via the liable route was reported by Takeichi et al. [5]. They found that 50% dense polyimide had a comparable elastic modulus (2.64 GPa) to that of dense solid (2.53 GPa) while 80% dense polyimide had a higher elastic modulus (3.21 GPa). The number of cells along the film thickness in Han's and Takeichi's studies was well beyond the number where edge effects [6] would be significant. Instead, the stiffening observed in these studies may be associated with size-stiffening arising from the small size of the cell struts.

Size-stiffening [7, 8] and hardening [9–14] were experimentally observed in nanoindentations as well as in

micro-rod torsion and micro-beam bending and were attributed to non-negligible strain gradients. Ashby et al. [15] recognized that strain gradients can lead to geometrically necessary deformations in materials. In metals, strain gradients generate additional geometrically necessary dislocations; in polymers, strain gradients generate geometrically necessary kinks. In both cases, the yield stresses are observed to increase with the strain gradient in nanoindentations [10, 16]. In polymers, the normalized bending stiffness of epoxy beams, which is expected to be independent of the normalized beam thickness, was found to exhibit an inverse square of the thickness dependence predicted by higher-order strain gradient elasticity. The increase is associated with a bending parameter, b_h, which, according to higher-order elasticity, depends on the higher-order material parameters, l_0, l_1, and l_2, where l_0 is associated with dilatation gradients, l_1 is associated with stretch gradients, and l_2 is associated with rotation gradients. Since macromolecular chains in polymers deform via rotation, only rotation gradients would be active and only l_2 would be non-zero among the higher-order material parameters in polymers. Experiments on the creep deflection of epoxy beams confirmed that only a single l_2 is required to account for the size-dependent stiffening in the elastic and creep deflection behaviors of epoxy beams [17]. This means that the spring and dashpot elements in the higher-order standard viscoelastic model have the same l_2. Since both time-independent elastic and time-dependent creep deformations are chain rotation based, this means that the dependence is geometric in character and is associated with rotation gradients.

Physically, the behavior can be understood using Ashby's model for geometrically necessary dislocations under pure bending. Instead of additional geometrically necessary dislocations, additional geometrically necessary rotations are generated by the strain gradients along the thickness direction of the beam upon bending of thin beams. The higher-order stiffening behavior can be described using higher-order theories such as micropolar media and micromorphic media [18]. The micropolar theory was reformulated by Fleck and Hutchinson [9, 19] to explain plastic hardening in the torsion of micron-sized copper wires. In this couple stress theory, one additional length parameter for the rotation strain gradient was introduced. Subsequently, Fleck and Hutchinson developed the strain gradient plasticity theory that incorporated full second-order derivatives of displacement [20] on the basis of earlier works [21–24]. Lam et al. [7] extended the strain gradient theory to the elastic range by recomposing the strain gradients into dilatation, stretch and rotation parts. Beam bending solutions were derived on the basis of the new theory and good agreements with experiments were obtained. For polymers undergoing small deformation, the macromolecular chains deform via bond rotation and only the rotation gradients are active. The deformation behavior can be described by the couple stress theory with a single higher-order material length-scale parameter, l_2, to account for the contributions from rotation gradients.

In this investigation, finite-element modeling (FEM) of couples stress solids was developed and benchmarked. Subsequently, the stiffening behaviors of cellular solids with different cell arrangements and densities were modeled using FEM. We show in this study that the elastic modulus decreases as a function of decreasing density but then increases with higher-order stiffening. The conditions required for this U-turn in the elastic modulus are described.

Higher-order mechanics

According to conventional elasticity theory, the deformation energy density, w, is a function of strain

$$w = \frac{1}{2}k\varepsilon_{ii}\varepsilon_{jj} + \mu\varepsilon'_{ij}\varepsilon'_{ij}, \tag{1}$$

where ε'_{ij} is a deviatoric strain,

$$\varepsilon'_{ij} = \varepsilon_{ij} - \frac{1}{3}\varepsilon_{mm}\delta_{ij}, \tag{2}$$

and k and μ are the bulk and shear modulus, respectively. When contributions from strain gradients are included, the deformation energy is a function of both the strain tensor, ε_{ij}, and the strain gradient tensor, η_{ijk},

$$\eta_{ijk} = \partial_{ij}u_k, \tag{3}$$

where ∂_i is the forward gradient operator and u_k is the displacement vector. According to Lam et al. [7], the deformation energy density for linear elastic centersymmetric isotropic materials is

$$w^{SG} = \frac{1}{2}k\varepsilon_{ii}\varepsilon_{jj} + \mu\left(\varepsilon'_{ij}\varepsilon'_{ij} + l_0^2\gamma_i\gamma_i + l_1^2\eta^{(1)}_{ijk}\eta^{(1)}_{ijk} + l_2^2\chi^s_{ij}\chi^s_{ij}\right), \tag{4}$$

where γ_i, $\eta^{(1)}_{ijk}$, and χ^s_{ij} are the dilatation gradient vector, the deviatoric stretch gradient tensor, and rotation gradient tensor, respectively. The strain gradient tensors are defined as

$$\gamma_i = \eta_{mim}, \tag{5}$$

$$\begin{aligned}
\eta^{(1)}_{ijk} &= \eta^s_{ijk} - \eta^{(0)}_{ijk} \\
\eta^s_{ijk} &= \frac{1}{3}(\eta_{ijk} + \eta_{jki} + \eta_{kij}) \\
\eta^{(0)}_{ijk} &= \frac{1}{5}(\delta_{ij}\eta^s_{mmk} + \delta_{jk}\eta^s_{mmi} + \delta_{ki}\eta^s_{mmj}) \\
\eta^s_{mmk} &= \frac{1}{3}(\eta_{mmk} + 2\eta_{kmm}),
\end{aligned} \tag{6}$$

where δ_{ij} is the Kronecker symbol. l_0, l_1, and l_2 are independent material parameters associated with dilatation gradients, deviatoric stretch gradients, and rotation gradients,

respectively. The corresponding higher-order stresses can be derived from Eq. 4 by taking the partial derivatives of the energy with respect to ε_{ij}, γ_i, $\eta^{(1)}_{ijk}$, and χ^s_{ij}. The stresses are

$$\begin{aligned} \sigma_{ij} &= k\delta_{ij}\varepsilon_{mm} + 2\mu\varepsilon'_{ij} \\ p_i &= 2\mu l_0^2\gamma_i \\ \tau^{(1)}_{ijk} &= 2\mu l_1^2\eta^{(1)}_{ijk} \\ m^s_{ij} &= 2\mu l_2^2\chi^s_{ij}, \end{aligned} \tag{7}$$

where σ_{ij} is the stress associated with strain, and p_i, $\tau^{(1)}_{ijk}$, m^s_{ij} are higher-order stresses associated with the dilatation, deviatoric stretch, and the symmetric rotation gradient, respectively. Details of the strain gradient mechanics are given in a paper by Lam et al. [7].

In polymers, when the equilibrium of the moments of couples is enforced on the rotations, only the symmetric parts of the rotation gradient's contributions are non-zero and finite [25]. As a result, the deformation energy density, w^{cs}, for couple stress solids can be simplified to

$$w^{\mathrm{CS}} = \frac{1}{2}k\varepsilon_{ii}\varepsilon_{jj} + \mu\left(\varepsilon'_{ij}\varepsilon'_{ij} + l_2^2\chi^s_{ij}\chi^s_{ij}\right), \tag{8}$$

where l_2 is a material length scale parameter, χ^s_{ij} is the symmetric part of the rotation strain gradient, χ_{ij}, and is defined as

$$\chi^s_{ij} = \frac{1}{2}(\chi_{ij} + \chi_{ji}), \tag{9}$$

where

$$\chi_{ij} = \frac{1}{2}e_{ipq}\eta_{jpq} \tag{10}$$

and e_{ijk} is an alternating tensor. For this case, where only rotation gradients are active, all higher-order stress vanishes except for m^s_{ij}.

The finite-element method with higher-order effect

Modeling approach

The displacement field in conventional mechanics can be used as a displacement field template for strain gradient models in FEM. Mathematically, the higher-order (couple stress) equilibrium equation is

$$\partial_i\sigma_{ik} - \frac{1}{2}e_{jlk}\partial_{il}m^s_{ij} - \partial_{ik}p_i - \partial_{ij}\tau^{(1)}_{ijk} + f_k = 0, \tag{11}$$

where f_k is the gravitation force. For small deformation, the strain is

$$\varepsilon_{ij} = \frac{1}{2}\left(\partial_j u_i + \partial_i u_j\right). \tag{12}$$

By incorporating the constitutive relationships (7) with the deformation Eqs. 3, 5–6, and 9–10, the equilibrium equation (ignoring body forces) can be expressed in terms of displacements as

$$\begin{aligned} &\left(k + \frac{2}{3}\mu\right)\partial_j\left(u_{m,m}\right) + \mu\nabla^2 u_j \\ &\quad - \mu\nabla^2\left[H_1\partial_j\left(u_{m,m}\right) + H_2\nabla^2 u_j\right] = 0, \end{aligned} \tag{13}$$

where ∇^2 is a Laplace differential operator, and

$$H_1 = 2l_0^2 - l_2^2 + \frac{4}{15}l_1^2, \tag{14}$$

$$H_2 = l_2^2 + \frac{8}{15}l_1^2 \tag{15}$$

are material parameters dependent on l's. In a couple stress solid, l_0 and l_1 are negligible, and Eq. 13 becomes

$$\begin{aligned} &\left(k + \frac{2}{3}\mu\right)\partial_j\left(u_{m,m}\right) + \mu\nabla^2 u_j \\ &\quad - \mu l_2^2\nabla^2\left[\nabla^2 u_j - \partial_j\left(u_{m,m}\right)\right] = 0, \end{aligned} \tag{16}$$

in which the conventional Lame equation,

$$\left(k + \frac{2}{3}\mu\right)\partial_j\left(u_{m,m}\right) + \mu\nabla^2 u_j = 0, \tag{17}$$

is embedded. The conventional displacement fields that satisfy this conventional Lame equation will also satisfy the higher-order equilibrium and governing equations in the bulk of the domain. This is demonstrated in the higher-order torsion and bending solutions [7, 16] that are functionally identical to the conventional solutions, except for an inverse squared dependence on the beam thickness and the rod's diameter, which account for the higher-order dependence. This means that at a constant beam deflection or twist, the higher-order solution and the conventional solution share similar displacement fields everywhere except at the boundary where the strain gradients affect the boundary behavior. However, Lam et al. [7] have shown that the effect of strain gradients at the fixed end of a bending cantilever is minor. In short beams (a ratio of length to thickness equal to 5), the error due to higher-order boundary conditions is less than 11%, which is less than typical experimental error. The recognition of this enables the use of displacement fields that satisfy the conventional Lame equation as a displacement field template in the development of the higher-order solution.

Deformation energy and FEM formulation

In elastic materials, the total potential energy, Π, is

$$\Pi = U^{\mathrm{c}} + U^{\mathrm{h}} - W^{\mathrm{c}} - W^{\mathrm{h}}, \tag{18}$$

where U^{c} is the conventional elastic energy, U^{h} is high-order (couple stress) deformation energy, and W^{c} and W^{h} are the work done by conventional external forces and

high-order external forces, respectively. U^{c} and U^{h} can be determined from the displacement field in FEM, which is obtained by solving the conventional stress equilibrium equations with corresponding boundary conditions. The discrete equilibrium equations in an element are

$$[K_e]\{q_e\} = \{P_e\}, \tag{19}$$

where $\{q_e\}$ and $\{P_e\}$ are the nodal displacement and nodal force, respectively. $[K_e]$ is the element stiffness matrix,

$$[K_e] = \int_{V_e} [B]^{T}[C][B]\mathrm{d}V, \tag{20}$$

where $[B]$ is the strain-displacement matrix and $[C]$ is the elastic matrix. The nodal displacement is obtained by solving the equilibrium equations. The displacement inside an element is deduced by interpolation of the nodal displacements,

$$u_i = \sum_{r=1}^{M} N^r q_i^r, \tag{21}$$

where u_i denotes the displacement component, N^r is the shape function of node r, M is the number of nodes in the element, and q_i^r is the nodal displacement component value of node r. The strain field is

$$\varepsilon_{ij} = \frac{1}{2}\sum_{r=1}^{M}\left[q_i^r(\nabla_j N^r) + (\nabla_i N^r)q_j^r\right], \tag{22}$$

where the gradient operator, ∇_i, is

$$\nabla_i = \frac{\partial}{\partial x_i}. \tag{23}$$

The corresponding strain gradient field is

$$\eta_{ijk} = \sum_{r=1}^{M}\left[\nabla_i(\nabla_j N^r)\right]q_k^r. \tag{24}$$

The invariant strain gradient tensor components can be derived from Eq. 9–10 and 5–6; and the stresses and high-order stresses can be obtained using Eq. 7. Using the Gaussian numerical integral method, the deformation energy in an element is calculated from

$$we^{CS} = \int_{V_e} w^{CS}\mathrm{d}V \tag{25}$$

for couple stress solids, where w^{CS} is defined in Eq. 8. The total deformation energies of the structure are

$$U^{CS} = U^{c} + U^{h} = \sum_{s=1}^{L_e} we^{CS}, \tag{26}$$

where L_e denotes the total element number in the structure. By noting that $\delta\Pi = 0$, the applied force for the higher-order case can be computed numerically using

$$F_i^I = \frac{\delta U^{CS}}{\delta u_i^I}, \tag{27}$$

where I denotes the specific force and the displacement at the same location. The total force for the structure is simply

$$F_i = \sum_{I=1}^{K} F_i^I. \tag{28}$$

Using this procedure, three-dimensional 8-node and 20-node finite elements were constructed to simulate the deformation behavior of higher-order solids. Beam bending models and rod torsion models were developed. The results were benchmarked with analytical solutions and experimental results and good agreements were obtained (Appendix 1). The benchmarked method is used to examine the deformation of cellular solids below.

Stiffening behavior in nanoporous cellular solids

At a fixed density, the elastic modulus of cellular solids is independent of the strut size, but it becomes size-dependent if there is stiffening. We shall examine the stiffening effect as a function of the strut size in simple cubic (SC) and face-centered cubic (FCC) cellular solids (Fig. 1).

The tensile deformation behaviors of porous films with and without stiffening were analyzed using the finite-element method outlined in the previous section. Films with seven-unit length, three-unit width, and two-unit thickness were built and loaded along the length direction. In the simulations, the porosity was varied from $\sim$10% to $\sim$45%.

The effects of l_2/L on the elastic modulus of the films are shown in Fig. 2. The curves show that doubling l_2/L from 0.3 to 0.6 can approximately double the stiffening in both SC and FCC films, although the stiffening in the FCC films is higher by approximately 30% relative to that in the SC films at the same density.

The stiffening as a function of the relative density is shown in Fig. 3a for SC film. The results show that the stiffness can become equal or higher than the stiffness of the fully dense solid (Fig. 3) with half the density.

Discussion

The notion of a porous solid having higher stiffness than a dense solid has been recognized in porous polyimide films with nanostruts. These films were experimentally observed to have an elastic stiffness that was 12% higher than that of the solid polyimide film. The FEM results in this study showed that the significantly higher stiffness is present if the cellular solid is engineered with a proper

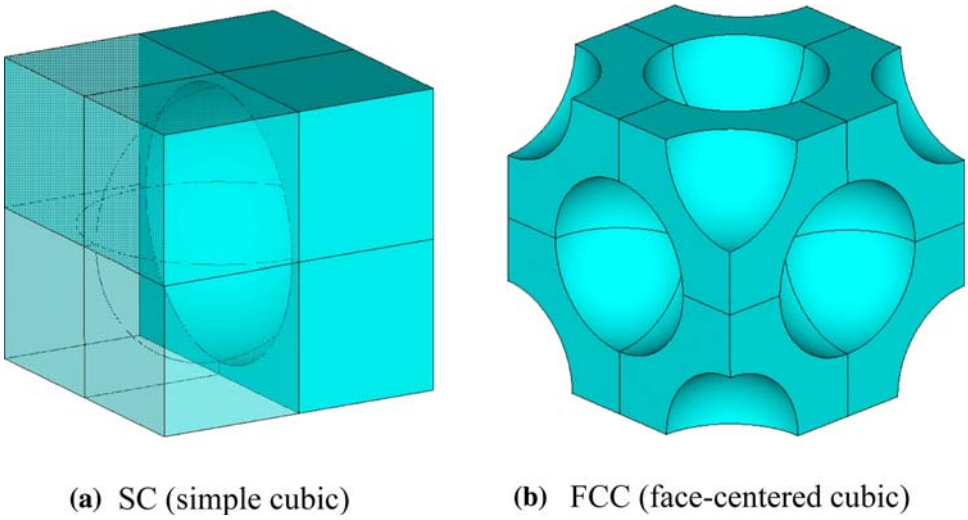

Fig. 1 Unit cells for modeling porous films

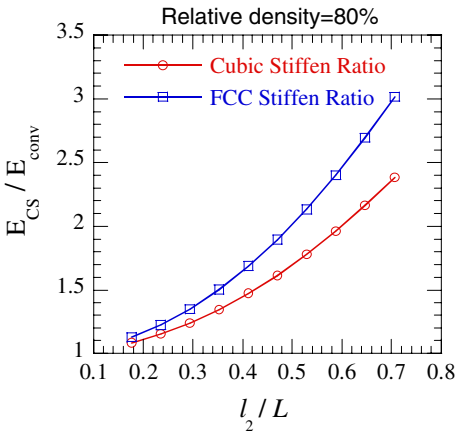

Fig. 2 The normalized E varies with l_2/L in SC and FCC units

microarchitecture, i.e., l_2/L and the density. Significant stiffening occurs when the higher-order length scale parameter, l_2, is on the order of the size of the cell L. The fact that nanostrutted polyimide is observed to have stiffening suggests that the l_2 for polyimide is in the nanometer range. More investigations are needed to characterize the l_2 of materials such that the strut size in cellular solids can be tailored to be on the order of l_2 to engender high stiffness in the cellular solid at half the weight.

Conclusions

The higher-order finite-element method was developed upon recognition that the displacement field satisfying the conventional Lame governing equations for elastic solids can also serve as a displacement field template to satisfy the higher-order Lame equation. A modeling method to account for the higher-order deformation was developed and this approach was shown to be in good agreement with experimentally benchmarked bending and torsion solutions. The developed method was used to analyze the higher-order stiffening behavior of cellular solids. The results showed that the elastic modulus of porous solid

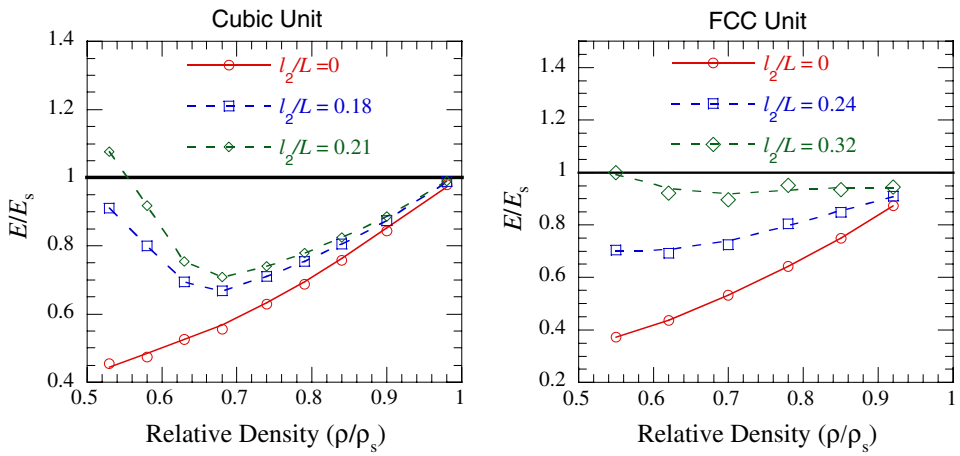

(a) SC (simple cubic) units **(b)** FCC (face-centered cubic) units

Fig. 3 The relative elastic modulus as a function of the relative density of porous solids

that initially decreases with increasing porosity will reverse and then increase when there is significant higher-order stiffening. This suggests that a proper selection of the higher-order material properties, micro-cellular architecture, and density can generate porous solids that are equally stiff as dense solids, but with half the weight.

Acknowledgement Jun Wang acknowledges support from the Shanghai Leading Academic Discipline Project (Project Number: B113). DCC Lam acknowledges funding support (615007, 615505, HKUST6190/03E) from the Research Grants Council of the HKSAR, China.

Appendix I: FEM verification

Higher-order strain gradient solutions are available for torsion, pure bending, and cantilever bending. A two-dimensional eight-node high-order element was used to model the higher-order deformation behavior in cantilever bending and pure bending. A three-dimensional 20-node high-order element was used in the torsion case.

Bending of micro-beams

Pure bending and cantilever bending cases are sketched in Fig. 4. For the pure bending case with small deformation, an analytical solution was developed [22]. The ratio of the total moment to the conventional moment in pure bending of a beam with elasticity is

$$\frac{M}{M_0} = 1 + 6(1-\nu)\left(\frac{l_2}{h}\right)^2. \tag{29}$$

In the absence of higher-order effects, M reverts to the conventional M_0. A comparison of the moment ratio between FEM and the analytical solution in Eq. 29 is shown in Fig. 5.

The bending rigidities for beams with different thicknesses are plotted in Fig. 6. These results show that the FEM results for pure bending and for cantilever bending, where there is shear, are in good agreement with experimentally benchmarked analytical models.

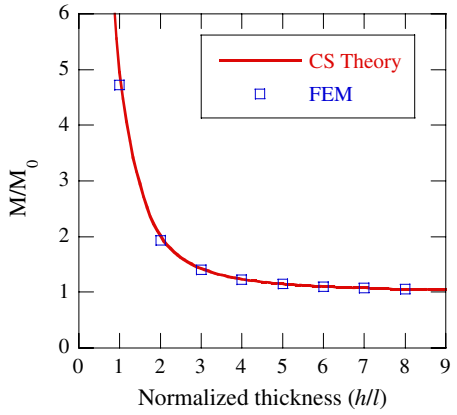

Fig. 5 Comparison of normalized moments between FEM results and analytical solutions of pure bending

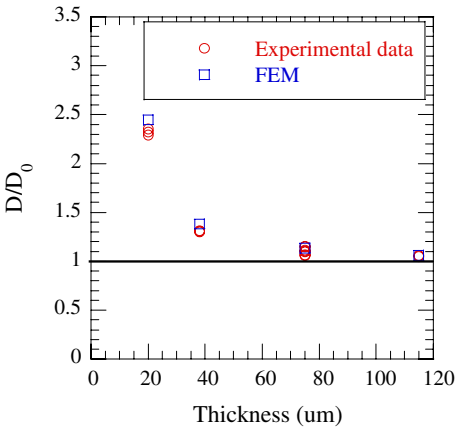

Fig. 6 Comparison of the normalized rigidity from experiments [7] and FEM results

Torsion

The behavior of micro-rod torsion was also examined and its typical mesh is illustrated in Fig. 7. The solution for a couple stress solid rod under torsion was derived in [25] and is given as

$$Q = Q_0\left[1 + 6\left(\frac{l_2}{r}\right)^2\right], \tag{30}$$

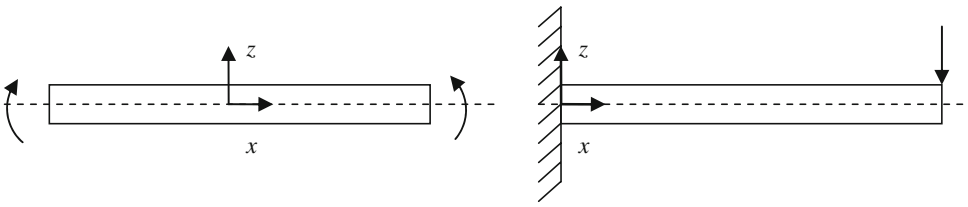

Fig. 4 Sketches of two kinds of micro-beam bending

(a) Pure bending **(b)** Cantilever bending

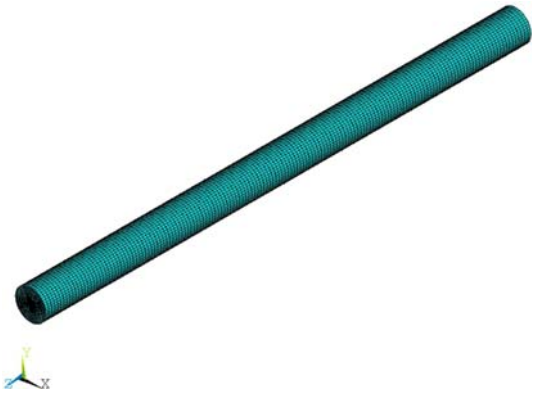

Fig. 7 A typical micro-rod mesh for FEM

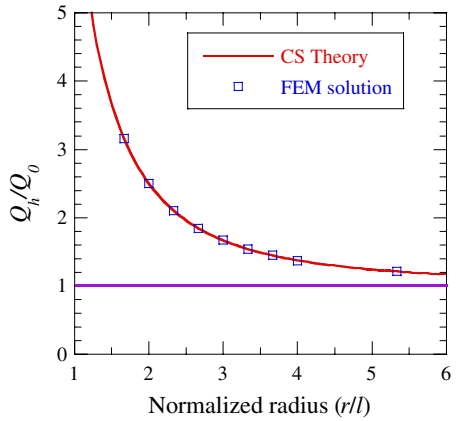

Fig. 8 Comparison of the normalized torque in micro-rod between FEM results and CS theory

where Q and Q_0 are the couple stress torque and conventional torque, respectively, and r is the radius of the micro-rod. The FEM results are consistent with the analytical solution according to Fig. 8.

References

1. Ashby MF (2000) Metal foams: a design guide. Butterworth-Heinemann, Boston
2. Gibson LJ, Ashby MF (1982) Proc R Soc Lond 382:43
3. Andrews EW, Gioux G, Onck P, Gibson LJ (2001) Int J Mech Sci 43:701
4. Han SH, Do JS, Kader MA, Lee JH, Lee MH, Nah CW (2004) Polym Adv Technol 15:370
5. Takeichi T, Zuo M, Ito A (1999) High Perform Polym 11:1
6. Tekoglu C, Onck PR (2005) J Mater Sci 40:5911. doi:10.1007/s10853-005-5042-5
7. Lam DCC, Chong ACM, Yang F, Wang J, Tong P (2003) J Mech Phys Solids 51:1477
8. McFarland AW, Colton JS (2005) J Micromech Microeng 15:1060
9. Fleck NA, Muller GM, Ashby MF, Hutchinson JW (1994) Acta Metall Mater 42:475
10. Lam DCC, Chong ACM (1999) J Mater Res 14:3784
11. Ma O, Clarke DR (1995) J Mater Res 10:853
12. Nix WD (1989) Metall Trans A 20:2217
13. Poole WJ, Ashby MF, Fleck NA (1996) Scr Mater 34:559
14. Stolken JS, Evans AG (1998) Acta Metall Mater 46:5109
15. Ashby MF (1970) Philos Mag 21:399
16. Chong ACM, Yang F, Lam DCC, Tong P (2001) J Mater Res 14:1052
17. Lam DCC, Keung LH, Tong P (2008) J Mater Sci Eng A (submitted)
18. Cermal EA (1976) Continuum physics. Academic Press, New York
19. Fleck NA, Hutchinson JW (1993) J Mech Phys Solids 41:1825
20. Fleck NA, Hutchinson JW (1997) Adv Appl Mech 33:295
21. Toupin RA (1962) Arch Ration Mech Anal 11:385
22. Koiter WT (1964) Proc K Ned Akad Wet (B) 67:17
23. Mindlin RD (1964) Arch Ration Mech Anal 16:51
24. Mindlin RD (1965) Int J Solids Struct 1:417
25. Yang F, Chong ACM, Lam DCC, Tong P (2002) Int J Solids Struct 39:2731